MICROMECHANICAL MODELS FOR TEXTILE COMPOSITES*

Bhavani V. Sankar
and
Ramesh V. Marrey
Center for Studies of Advanced Structural Composites
University of Florida
Gainesville, FL

1. SUMMARY

Numerical and analytical micromechanical models are presented to predict the thermo-elastic behavior of a textile composite. In the numerical model, the unit-cell is discretized with finite elements, and periodic boundary conditions are imposed between opposite faces of the unit-cell. For a thin textile composite, stress gradients effects through the thickness are demonstrated. The consequent difference in the stiffness and strength behavior of thick and thin composites are discussed. The numerical model is implemented to predict the 3-D thermo-elastic constants for a thick textile composite, and the plate thermo-mechanical properties for a thin textile composite. The numerical model is extended to compute the thermal residual microstresses due to processing and to predict the composite failure envelopes. An analytical model - Selective Averaging Method (SAM) - is proposed, which is based on a judicious combination of stiffness and compliance averaging to estimate the 3-D elastic constants. Both the models are tested and verified for several examples by comparing the stiffness properties with elasticity solutions and available results.

2. INTRODUCTION

The increasing demand for lightweight yet strong and stiff structures has lead to the development of fiber reinforced composites. These materials are not only used in the aerospace industry but also in variety of commercial applications like automobile, marine and biomedical applications. However the manufacture of fibrous laminated composites from prepregs is labor intensive. Besides, fibrous laminated composites lack through the thickness reinforcement, and hence have poor interlaminar shear strength. Recent developments in textile technology shows some promise in overcoming the above limitations. Three-dimensional woven and braided composites provide multidirectional reinforcement, thus enhancing the strength and stiffness in the thickness direction. Textile manufacturing processes such as weaving and braiding in conjunction with resin transfer molding are also suitable for the production of intricate structural forms at a reduced turn-round time.

With the advancements in aforementioned technologies there is a need to develop scientific methods of predicting the performance of the composites made using the above processes. There are numerous variables involved in textile processes besides the choice of the fiber and matrix materials. This, for example, includes the number of filaments in the yarn specified by the yarn linear density and the yarn architecture within the unit-cell determined by the type of weaving or braiding processes. Thus there is a need for analytical/numerical models to study the effect of these variables on the textile composite behavior. Ideally a structural engineer would like to model textile composites as a homogeneous anisotropic material - preferably orthotropic - so that the structural computations can be simplified, and also the existing computer codes can be used in the design. This would require the prediction of the effective (macroscopic) properties of the composites from the constituent material (microscopic) characteristics such as fiber and matrix properties, fiber-matrix interface characteristics and the fiber architecture. This is possible if we assume that there is a representative volume element (RVE) or an unit-cell that repeats its self throughout the volume of the composite, which seems to be true in the case of textile composites. Ishikawa and Chou (1982; 1983a; 1983b), Yang and Chou (1987), Ma, Yang and Chou (1986), have proposed several models for estimating the thermoelastic and mechanical properties of woven and braided composites. Yoshino and Ohtsuka (1982), Dasgupta et al. (1990) and Whitcomb (1991) analyzed the unit-cell of textile composites using three-dimensional finite elements to predict the overall macroscopic behavior of the composites. Their models can be used to predict both stiffness and strength properties. In the present paper, we have demonstrated numerical models to predict the stiffness and strength behavior of textile composites. An approximate analytical method is also described to estimate the stiffness properties of a textile composite.

3. FINITE ELEMENT MODELS FOR THERMO-MECHANICAL PROPERTIES

In this section, we demonstrate micromechanical models utilizing finite elements to predict the effective stiffness properties and coefficients of thermal expansion (CTE's) for a textile composite. The macroscopic properties of the composite are determined at a scale much larger than the dimensions of the unit-cell, but comparable to the dimensions of the structural component. The average stresses at a point at the structural scale will be called the macroscopic stresses or macrostresses. The actual stresses at a point at the continuum level will be called the microscopic stresses or microstresses.To distinguish the macroscopic deformations and stresses from their microscale counterparts - a superscript "M" will be used to denote the macroscopic deformations and stresses.

3.1 Unit-Cell Analysis for Three-Dimensional Elastic Constants

The unit-cell analysis assumes that the material is subjected to a uniform state of strain in the macroscopic sense. The average stresses required to create such a state of strain is computed from the finite element model of the unit-cell. In the microscale, all unit-cells have

identical stress and strain fields. Continuity of stresses across the unit-cell then requires that tractions be equal and opposite at corresponding points on opposite faces of the unit-cell. Since the displacement gradients are constant for a homogeneous deformation, the displacements at corresponding points on opposite faces of the unit-cell differ only by a constant.

Consider a rectangular parallelepiped as the unit-cell of the three-dimensional textile composite. The edges of the unit-cell are assumed to be parallel to the coordinate axes x_1, x_2 and x_3, with unit-cells repeating in all three directions. The length of the unit-cell in the x_i direction is defined as L_i. On the macroscale the composite is assumed to be homogeneous and orthotropic and the composite behavior is characterized by the following constitutive relation :

$$
\left\{
\begin{array}{c}
\sigma_{11}^M \\
\sigma_{22}^M \\
\sigma_{33}^M \\
\tau_{23}^M \\
\tau_{31}^M \\
\tau_{12}^M
\end{array}
\right\}
=
\begin{bmatrix}
C_{11} & C_{12} & C_{13} & C_{14} & C_{15} & C_{16} \\
       & C_{22} & C_{23} & C_{24} & C_{25} & C_{26} \\
       &   & C_{33} & C_{34} & C_{35} & C_{36} \\
       & symm. &   & C_{44} & C_{45} & C_{46} \\
       &   &   &   & C_{55} & C_{56} \\
       &   &   &   &   & C_{66}
\end{bmatrix}
\left(
\left\{
\begin{array}{c}
\epsilon_{11}^M \\
\epsilon_{22}^M \\
\epsilon_{33}^M \\
\gamma_{23}^M \\
\gamma_{31}^M \\
\gamma_{12}^M
\end{array}
\right\}
-
\left\{
\begin{array}{c}
\alpha_1^s \\
\alpha_2^s \\
\alpha_3^s \\
\alpha_{23}^s \\
\alpha_{31}^s \\
\alpha_{12}^s
\end{array}
\right\}
\Delta T^M
\right)
\qquad (1)
$$

where $\{\sigma^M\}$ and $\{\varepsilon^M\}$ are the macroscale stresses and strains respectively; $\{\alpha^s\}$ and $[C]$ are the macroscale CTE's and orthotropic elasticity matrix to be determined; ΔT^M is a uniform temperature difference throughout the unit-cell.

3.1.1 Periodic Boundary Conditions

The periodic BC's consist of the periodic displacement boundary conditions which ensure the compatibility of displacements on opposite faces of the unit-cell, and the periodic traction boundary conditions to enforce the continuity of stresses. A macroscopically homogeneous deformation can be represented as

$$
u_i^M = H_{ij} x_j \qquad i,j=1,2,3 \qquad (2)
$$

where H_{ij} are the displacement gradients. Then the periodic displacement boundary conditions to be imposed on the faces $x_i=0$ and $x_i=L_i$ are

$$
u_i(L_1,x_2,x_3) - u_i(0,x_2,x_3) = H_{i1}L_1
$$

$$
u_i(x_1,L_2,x_3) - u_i(x_1,0,x_3) = H_{i2}L_2 \qquad (3)
$$

$$
u_i(x_1,x_2,L_3) - u_i(x_1,x_2,0) = H_{i3}L_3
$$

The traction boundary conditions to be imposed on the faces $x_i=0$ and $x_i=L_i$ are

$$F_i(L_1,x_2,x_3) = -F_i(0,x_2,x_3)$$

$$F_i(x_1,L_2,x_3) = -F_i(x_1,0,x_3)$$

$$F_i(x_1,x_2,L_3) = -F_i(x_1,x_2,0)$$

(4)

The above periodic BC's are imposed in the finite element model by using multi-point constraint elements or by using transformation equations to eliminate the constrained displacements (Cook et al., 1989). Both methods require a finite element model with corresponding nodes on opposite faces of the unit-cell.

3.1.2 Determination of Three-Dimensional Elastic Constants and CTE's

The unit-cell is discretized with three-dimensional finite elements such that opposite faces of the unit-cell have identical nodes. Periodic displacement and traction boundary conditions are enforced between the corresponding nodes. The periodic displacement BC's are imposed such that only one of the components of the macroscopic strains is non-zero; and the uniform temperature difference ΔT^M is set to zero. Then, the difference in displacements between corresponding points on opposite faces of the unit-cell will be equal to that in a homogenous continuum subject to the same deformation. The average stresses (macroscopic stresses) required to create such a deformation are obtained from the finite element results. Substituting the macroscopic stresses and strains in the composite constitutive relation Eqn. (1) the stiffness coefficients in the column corresponding to the non-zero strain can be evaluated. This procedure is repeated for other macroscopic strain components (keeping the temperature difference zero) to obtain the entire stiffness matrix $[C]$. The orthotropic elastic constants of the composite material can be easily determined by inverting the stiffness matrix, and comparing the compliance coefficients with that of an orthotropic material.

To compute the six CTE's, a finite temperature change T_o is applied to all the elements in the unit-cell; and periodic displacement BC's are imposed such that all the macroscopic strain components are zero. Then the composite constitutive relation Eqn. (1) will reduce to

$$\{\sigma^M\} = -[C]\{\alpha^s\}\, T_o$$

(5)

The macroscopic stresses for such a deformation are computed as described below. Knowing the stiffness matrix $[C]$, the composite CTE's are found as

$$\{\alpha^s\} = -\frac{1}{T_o}[C]^{-1}\{\sigma^M\}$$

(6)

Table 1 presents the non-zero displacement BC's imposed on the unit-cell to obtain $[C]$ and the CTE's $\{\alpha^s\}$.

The macroscale stresses for a given deformation state can be found by one of the following two methods. In the first method, the macroscale stresses are obtained by averaging the nodal forces on each face of the unit cell. For example, the macroscale $\sigma_{11}{}^M$ can be

obtained as

$$\sigma_{11}^{M} = \frac{1}{L_2 L_3} \Sigma_n F_1^{(n)}(L_1, x_2, x_3) \qquad (7)$$

where $F_1^{(n)}$ is the nodal force in the x_1 direction at the nth node, and Σ_n denotes summation over all nodes on the face $x_1 = L_1$. Alternately, the macroscopic stresses can be computed by volume-averaging the corresponding microstress component in the unit-cell. Then the macroscale σ_{11}^{M} is obtained as

$$\sigma_{11}^{M} = \frac{1}{V} \int_V \sigma_{11}(x, y, z) dV \qquad (8)$$

where V is the volume of the unit-cell. The microstresses are computed at the quadrature points, and numerically integrated over the volume in each element of the unit-cell.

3.1.3 Results and Discussion for 3-D Elastic Constants and CTEs

The above procedure was demonstrated for the following materials:

Example 1.   isotropic material

Example 2.   bimaterial medium - both materials are assumed isotropic

Example 3.   unidirectional composite with identical poisson ratios for fiber and matrix - fiber and matrix materials are isotropic

Example 4.   unidirectional composite with different poisson ratios for fiber and matrix - fiber and matrix materials are isotropic

Example 5.   plain-weave textile composite (yarn geometry and properties obtained from Dasgupta et al., 1990)

Example 6.   plain-weave textile composite (yarn geometry and properties obtained from Naik, 1994)

Example 7.   5-harness satin weave (yarn geometry and properties obtained from Naik, 1994)

For the textile composite examples, i.e, examples 5-7, the yarn is assumed to be transversely isotropic and the matrix material is assumed isotropic. The constituent material properties for the examples are listed in Table 2.

A 3-D finite element code called $\mu TE\chi$-20 (pronounced as *mutech*) was written and implemented for the seven examples to compute the homogeneous elastic constants and CTE's. The unit-cell was divided into uniform eight noded hexahedral elements. The element stiffness matrix (K^e) was formulated as

$$K^e = \int_{V^e} B^T CB \, dV^e$$

$$= \int_{-1}^{+1} \int_{-1}^{+1} \int_{-1}^{+1} B^T CB |J| \, d\xi \, d\eta \, d\zeta \qquad (9)$$

$$\approx \sum_{i=1}^{N} \sum_{j=1}^{N} \sum_{k=1}^{N} W_i W_j W_k B^T C(\xi, \eta, \zeta) B |J|$$

where V^e is the domain of the element, B is the strain-displacement transformation matrix, C

is the elasticity matrix, N is the number of Gauss points used for integration, W is the Gaussian integration weight factor and $|J|$ is the determinant of the Jacobian. The material property at each Gauss point (ξ,η,ζ) was determined, and the corresponding elasticity matrix was used to perform the volume integration. The element stiffness matrix thus represented the averaged properties of the constituent materials in that element. The computed elastic constants for the seven examples are listed in Tables 3-5.

The bimaterial medium consisted of two different layers of equal thickness in the xy-plane alternating in the z-direction (Fig. 1). The effective Youngs moduli, Poisson ratios and CTE's of the bimaterial medium were derived exactly as described below. The constitutive relation (considering only the normal stresses) for each layer was defined as

$$\begin{Bmatrix} \sigma_{xx}^i \\ \sigma_{yy}^i \\ \sigma_{zz}^i \end{Bmatrix} = \begin{bmatrix} C_{11}^i & C_{12}^i & C_{13}^i \\ C_{12}^i & C_{22}^i & C_{23}^i \\ C_{13}^i & C_{23}^i & C_{33}^i \end{bmatrix} \begin{Bmatrix} \epsilon_{xx}^i \\ \epsilon_{yy}^i \\ \epsilon_{zz}^i \end{Bmatrix} \qquad i=1,2 \tag{10}$$

where the superscript refers to the layer number. To derive C_{11}, C_{12} and C_{13} for the bimaterial medium, ϵ_{xx}^M was assumed as one; and ϵ_{yy}^M and ϵ_{zz}^M as zero. The assumption of $\epsilon_{zz}^M=0$ implied that $\epsilon_{zz}^1= -\epsilon_{zz}^2$. The following constraints were, in addition, imposed across the bimaterial interface :

$$\epsilon_{xx}^1 = \epsilon_{xx}^2 = \epsilon_{xx}^M$$

$$\epsilon_{yy}^1 = \epsilon_{yy}^2 = \epsilon_{yy}^M \tag{11}$$

$$\sigma_{zz}^1 = \sigma_{zz}^2 = \sigma_{zz}^M$$

From the above interfacial constraints and Eqn. (10), the stresses in each layer were computed. The stresses in the layers were volume-averaged to yield the corresponding macroscopic stresses, i.e, σ_{xx}^M, σ_{yy}^M and σ_{zz}^M. Since ϵ_{xx}^M was equal to unity, the computed macroscopic stresses were identical to the stiffness coefficients C_{11}, C_{12} and C_{13}. A similar procedure was followed to find the remaining stiffness coefficients and CTE's for the bimaterial medium. The inplane shear modulus of the bimaterial medium was computed as $G_{xy}= (G_1+ G_2)/2$ knowing that the shear strain was uniform in both layers. The isostress assumption was used to derive the transverse shear modulus as $G_{xz}= 2G_1G_2 / (G_1+G_2)$. It was found that $\mu TE\chi$-20 results were identical to the elasticity results for the bimaterial medium (Table 3).

Table 4 presents the elastic constants and CTE's for the two unidirectional composite examples. The unidirectional composite unit-cell is shown in Fig. 2. The unidirectional composite properties were compared with available analytical solutions. The rule of mixtures formulae were used to predict E_L and ν_{LT} ; the Halpin-Tsai equations (Halpin and Tsai, 1969) for E_T, G_{LT} and ν_{TT} and Schapery's expressions (Agarwal and Broutman, 1990) for the thermal

coefficients α_L and α_T. The relations for E_L, ν_{LT} and α_L are exact when the poisson ratios are identical for the fiber and the matrix. The reason for the discrepancy in example 3 is that a point-location subroutine in $\mu TE\chi$-20 identified a fiber volume fraction of 0.595, whereas the actual fiber volume fraction was 0.6.

The elastic constants for the three textile composite examples are presented in Table 5. Figures 3 & 4 illustrate the weave patterns for the plain-weave (examples 5 & 6) and the 5-harness satin weave (example 7) respectively. The properties for example 5 were compared with Dasgupta's results for an overall fiber volume fraction (V_f) of 0.26. The yarn properties were not specified in Dasgupta et al. (1990). So the rule of mixtures and Schapery's expressions were used to obtain the yarn properties from the given fiber and matrix properties. The $\mu TE\chi$-20 results for examples 6 and 7 were compared with TEXCAD - an approximate analytical method developed by Naik (1994). In both the examples the overall fiber volume fraction was 0.64. It must be noted that $\mu TE\chi$-20 will marginally under-predict the stiffness moduli - since the yarn cross-section in the numerical model is approximated as a polygon inscribed within the actual cross-sectional area. Consequently the yarn/fiber volume fraction in the numerical model will always be lesser that the theoretical volume fraction.

3.2 Stress Gradient Effects

The methods explained in Section 3.1 assume that the unit-cells exist in all the three directions. This will be true in the case of thick textile composites. However there are many applications in which thin composites are used. In fact in order to take advantage of the properties of composites, the structures have to be made of thin plate like members with stiffeners for load transfer. In such cases there will be fewer unit-cells in the thickness direction. Thus the free surface effects will be predominant. There will be severe stress gradients through the thickness, and they will have an influence on the apparent stiffness and strength of the structure.

The following simple example will illustrate the stress gradient effects on stiffness. Consider a layered medium consisting of alternating layers of materials of equal thickness with Young's moduli E_1 and E_2 respectively (Fig. 5a). Any micromechanical model would predict that the medium can be considered as a homogeneous orthotropic material at macroscale and also the effective Young's modulus in the longitudinal direction is $(E_1+E_2)/2$, and there would not be any bending-stretching coupling in the principal material direction. However, if we consider a bimaterial beam consisting of the same two materials (Fig. 5b), we will find that there is a bending-stretching coupling, and also the flexural rigidity cannot be predicted from the Young's modulus of the homogeneous orthotropic medium and the total beam thickness. The bimaterial beam has properties and behavior different from the corresponding infinite medium. This phenomenon is observed in the transverse shear behavior also (Sankar and Marrey, 1993). A similar behavior is also expected in thin textile composites where there are fewer unit-cells in the thickness directions, and the unit-cells are not subjected to a macroscopically homogeneous state of deformation as assumed in Section 3.1. The effect of stress gradients on stiffness and strength of thin textile composites are discussed

in Marrey and Sankar (1993a).

One method of overcoming the above difficulties in thin textile composites is to model the composite as a plate/beam, and compute the structural stiffness properties (eg., [A], [B] and [D] of the plate) directly from the unit-cell analysis instead of the continuum stiffness properties (Young's modulus, shear modulus etc.). In the following sub-sections we illustrate these concepts - first for a thin textile composite modeled as a beam, and then for a textile composite plate. The purpose of the beam model is to present the issues involved in computing the structural stiffness coefficients. Further the periodic BC's are different from those in the continuum model.

3.3 Unit-Cell Analysis for Beam Thermo-Mechanical Coefficients

The textile composite beam is assumed to be in the xz-plane with unit-cells repeating in the x-direction. A state of plane strain parallel to the xz-plane is assumed. On the macroscale it is assumed that the beam is homogeneous and its behavior can be characterized by the following beam constitutive relation :

$$\begin{Bmatrix} P \\ M \\ V \end{Bmatrix} = \begin{bmatrix} K_{11} & K_{12} & K_{13} \\ K_{12} & K_{22} & K_{23} \\ K_{13} & K_{23} & K_{33} \end{bmatrix} \left\{ \begin{Bmatrix} \epsilon_0^M \\ \kappa^M \\ \gamma_0^M \end{Bmatrix} - \begin{Bmatrix} \alpha_P \\ \alpha_M \\ \alpha_V \end{Bmatrix} \Delta T^M \right\} \tag{12}$$

where P, M and V are the axial force, bending moment and transverse shear force resultants respectively; $[K]$ is the symmetric matrix of beam stiffness coefficients; ϵ_0^M, κ^M and γ_0^M are the midplane axial strain, curvature and transverse shear strain respectively; α_P, α_V and α_M respectively are the thermal expansion, thermal shear and thermal bending coefficients. The midplane deformations are related to the midplane axial displacement u_0, transverse displacement w, and rotation ψ as:

$$\epsilon_0^M = \frac{\partial u_0}{\partial x}, \quad \kappa^M = \frac{\partial \psi}{\partial x}, \quad \gamma_0^M = \psi + \frac{\partial w}{\partial x} \tag{13}$$

Actually K_{11}, K_{12}, K_{22} and K_{33} are similar to the laminate stiffness coefficients A_{11}, B_{11}, D_{11} and $\kappa^2 A_{55}$ respectively. The beam constitutive relation in Eqn. (12) can also be expressed in terms of compliance coefficients as

$$\begin{Bmatrix} \epsilon_0^M \\ \kappa^M \\ \gamma_0^M \end{Bmatrix} = \begin{bmatrix} S_{11} & S_{12} & S_{13} \\ S_{12} & S_{22} & S_{23} \\ S_{13} & S_{23} & S_{33} \end{bmatrix} \begin{Bmatrix} P \\ M \\ V \end{Bmatrix} + \begin{Bmatrix} \alpha_P \\ \alpha_M \\ \alpha_V \end{Bmatrix} \Delta T^M \tag{14}$$

As discussed earlier, the unit-cell analysis assumes that all the unit-cells are subjected to identical stress and strain fields, for a given state of loading. This is true in the case of constant axial force (P) and constant bending moment (M) in the beam. However, when a shear force (V) is applied to the beam, the shear force will give rise to the building up of bending moment at every cross-section, such that $V = -(dM/dx)$. This situation created difficulties in estimating the shear stiffness of the beam accurately.

The detailed procedures for evaluating $[K]$ and the beam CTE's are explained in Sankar and Marrey (1993) and Marrey and Sankar (1993b). However the principles involved in finding the beam stiffness matrix $[K]$ are described briefly for the sake of completion. Three linearly independent deformations are applied to the unit-cell namely,

Case (i)   unit axial strain $(\varepsilon_0 = 1, \kappa = 0, \gamma_0 = 0)$
Case (ii)   unit curvature accompanied by transverse deflection such that the transverse shear strain was zero $(\varepsilon_0 = 0, \kappa = 1, \gamma_0 = 0)$
Case (iii)   unit transverse shear strain $(\varepsilon_0 = 0, \kappa = 0, \gamma_0 = 1)$

The periodic displacement boundary conditions for the three unit deformations are given in Table 6. The temperature change, ΔT, is assumed to be zero. The top and bottom surfaces of the unit-cell are considered as free surfaces. For each case, the axial force P, the bending moment at the center of the unit cell M, and the shear force V are computed. Since the bending moment varies linearly along the unit cell, the bending moment at the center will be the average of the bending moments at the left and right ends of the unit cell. By substituting the values of P, M and V in Eqn. (12), one can evaluate the stiffness coefficients.

3.3.1 Beam Results and Discussion

The procedures to obtain the beam coefficients were implemented for the following cases:
(a) an isotropic beam; (b) a bimaterial beam with isotropic layers of equal thickness; (c) a plain weave textile composite beam where the yarn is assumed to be transversely isotropic and the matrix is isotropic. The properties of the constituent materials for all the cases are listed in Table 7. The dimensions of the unit-cell and the yarn architecture for the textile beam were taken from Yoshino and Ohtsuka (1982). The same unit-cell dimensions (length of 3.6 mm and height 1.8 mm) were also used for the isotropic and bimaterial cases.

The unit-cell of the beam was discretized using eight-noded isoparametric plane strain finite elements. The finite element mesh for the isotropic unit-cell and the plain weave unit-cell were identical except that different material properties were used. The deformed plain weave unit-cell under various independent loading conditions is shown in Fig. 6.

The stiffness and thermal coefficients for the three beams examples are shown in Table 8. The results for the isotropic and bimaterial beams were compared to exact beam theory solutions. Exact shear correction factors - 0.833 for the isotropic beam and 0.555 for bimaterial beam were used in the beam theory solution to compute the shear stiffness (Whitney, 1973). It can be seen that the beam unit-cell analysis is able to predict the axial and bending stiffness coefficients $(K_{11}$ and $K_{22})$ very accurately. As expected the shear stiffness $(K_{33}$ or $A_{55})$ predictions have errors, but they are very minimal. The textile beam

stiffness coefficients were also estimated using a procedure similar to the mosaic model (Ishikawa and Chou, 1982). They are compared with the coefficients obtained from the unit-cell analysis as shown in Table 8. It can be seen that the mosaic model predicts K_{33} reasonably well. The reason for the lack of agreement in K_{11} and K_{22} can be attributed to the fact that a major portion of the yarn is modeled as a $0°$ laminate in the mosaic model, which tends to over-predict the axial and flexural stiffness.

The shear modulus of the plain-weave beam G_{xz} was found by imposing periodic boundary conditions between the top and bottom surfaces, and left and right ends of the unit-cell. This would yield the apparent shear stiffness as $G_{xz}h=5.53 \times 10^6$ Nm^{-1} - whereas the actual shear stiffness is 9.21×10^6 Nm^{-1} (K_{33} in Table 8). The Young's modulus of the textile beam E_x may be extracted from K_{11}, as K_{11}/h, which would yield $E_x=15.42$ GPa. If this value of E_x were used to predict the homogeneous flexural stiffness as $D_{11}=E_xh^3/12$, we would obtain D_{11} as 7.50 Nm - whereas the actual flexural stiffness is equal to 5.41 Nm. The same idea holds for the beam thermal coefficients also. The beam CTE's ,i.e, α_P, α_M and α_V cannot be predicted from the corresponding continuum CTE's. Table 9 shows the disagreement for the plain-weave example between the beam CTE's obtained directly, and the beam CTE's predicted from the corresponding continuum CTE's. It may be noted that the continuum model would always predict the thermal expansion coefficient α_P as α_x, and the thermal bending coefficient α_M as zero. This underscores the importance of the present analysis for predicting the beam stiffness properties for a thin textile composite directly.

3.4 Unit-Cell Analysis for Plate Thermo-Mechanical Coefficients

In this section we describe a procedure to find the stiffness and thermal properties of a textile fabric modeled as a structural composite plate. The textile composite plate is assumed to be in the xy-plane with unit-cells repeating in the x and y directions. The lengths of the unit-cell in the x- and y-directions are assumed to be a and b respectively and the unit-cell thickness as h. On the macroscale the plate is assumed to be homogeneous and the plate behavior is characterized by the plate constitutive relation:

$$
\begin{bmatrix}
A_{11} & A_{12} & A_{16} & B_{11} & B_{12} & B_{16} \\
A_{12} & A_{22} & A_{26} & B_{12} & B_{22} & B_{26} \\
A_{16} & A_{26} & A_{66} & B_{16} & B_{26} & B_{66} \\
B_{11} & B_{12} & B_{16} & D_{11} & D_{12} & D_{16} \\
B_{12} & B_{22} & B_{26} & D_{12} & D_{22} & D_{26} \\
B_{16} & B_{26} & B_{66} & D_{16} & D_{26} & D_{66}
\end{bmatrix}
\left(
\begin{Bmatrix}
\epsilon_{x0}^M \\
\epsilon_{y0}^M \\
\gamma_{xy0}^M \\
\kappa_x^M \\
\kappa_y^M \\
\kappa_{xy}^M
\end{Bmatrix}
-
\begin{Bmatrix}
\alpha_x^p \\
\alpha_y^p \\
\alpha_{xy}^p \\
\beta_x^p \\
\beta_y^p \\
\beta_{xy}^p
\end{Bmatrix}
\Delta T
\right)
=
\begin{Bmatrix}
N_x \\
N_y \\
N_{xy} \\
M_x \\
M_y \\
M_{xy}
\end{Bmatrix}
\tag{15}
$$

where ε_{io}^M, γ_{io}^M and κ_i^M are the midplane axial strain, shear strain and curvature; α_i^P and β_i^P are the plate thermal expansion and bending coefficients; N_i and M_i are the axial force and bending moment resultants respectively in the homogeneous plate. The midplane strains and curvatures are related to the midplane displacements and rotations as:

$$\epsilon_{x0}^M = \frac{\partial u_o}{\partial x}, \quad \epsilon_{y0}^M = \frac{\partial v_o}{\partial y}, \quad \gamma_{xy0}^M = \frac{\partial u_o}{\partial y} + \frac{\partial v_o}{\partial x} \tag{16}$$

$$\kappa_x^M = \frac{\partial \psi_x}{\partial x}, \quad \kappa_y^M = \frac{\partial \psi_y}{\partial y}, \quad \kappa_{xy}^M = \frac{\partial \psi_x}{\partial y} + \frac{\partial \psi_y}{\partial x} \tag{17}$$

3.4.1 Unit-Cell Boundary Conditions

The plate thermo-mechanical properties were obtained by modeling the unit-cell with eight-noded brick elements and subjecting the unit-cell to linearly independent deformations. The unit-cell was subjected to minimum support constraints to prevent rigid body rotation and translation. The top and bottom surfaces of the plate were assumed to be free of tractions. The faces $x=0$ and $x=a$ had identical nodes in the finite element model, and so did the pair of faces $y=0$ and $y=b$. The identical nodes on opposite faces of the unit cell were constrained to enforce the periodic BC's. The traction boundary conditions on the lateral faces of the unit-cell were:

$$F_i(a,y,z) = -F_i(0,y,z), \quad F_i(x,b,z) = -F_i(x,0,z), \quad i=x,y,z \tag{18}$$

The periodic displacement BC's enforced for the deformations are presented in Table 10.

3.4.2 Determination of Plate Stiffness Coefficients and CTE's

Linearly independent deformations are applied to the unit-cell such that only one of the six components of deformation is non-zero (first six cases in Table 10). The temperature difference is set to zero for all six cases. It must be noted that the applied deformations must ensure that the transverse shear strains, γ_{xz}^M and γ_{yz}^M are zero where

$$\gamma_{xz}^M = \psi_x + \frac{\partial w}{\partial x}$$

$$\gamma_{yz}^M = \psi_y + \frac{\partial w}{\partial y} \tag{19}$$

The force and moment resultants can be obtained by averaging the nodal forces on each face

of the unit cell. For example, on the face $x=a$ the force and moment resultants are computed using the relations:

$$N_x = \left(\frac{1}{b}\right) \sum_{i=1}^{n} F_x^{(i)}(a,y,z), \quad N_{xy} = \left(\frac{1}{b}\right) \sum_{i=1}^{n} F_y^{(i)}(a,y.z) \tag{20}$$

$$M_x = \left(\frac{1}{b}\right) \sum_{i=1}^{n} z\, F_x^{(i)}(a,y,z), \quad M_{xy} = \left(\frac{1}{b}\right) \sum_{i=1}^{n} z\, F_y^{(i)}(a,,y,z) \tag{21}$$

where $F_x^{(i)}$ and $F_y^{(i)}$ are the nodal forces in the x and y directions at the ith node and $'n'$ is the total number of nodes on the face. The force and moment resultants can also be computed by averaging the microstresses over the unit-cell volume. Then the resultants on the face $x=a$ are obtained as

$$N_x = \frac{1}{ab} \int_V \sigma_{xx}(x,y,z)dV \quad N_{xy} = \frac{1}{ab} \int_V \tau_{xy}(x,y,z)dV \tag{22}$$

$$M_x = \frac{1}{ab} \int_V z\,\sigma_{xx}(x,y,z)dV \quad M_{xy} = \frac{1}{ab} \int_V z\,\tau_{xy}(x,y,z)dV \tag{23}$$

Substituting the values of the deformation and the force resultants in the plate constitutive relation, Eqn. (15), the stiffness coefficients in the column corresponding to the non-zero deformation can be computed. This procedure is repeated for other deformation components to obtain all the stiffness coefficients.

To predict the CTE's, the plate unit cell is subject to a uniform temperature difference, given by $\Delta T = T_0$. In the finite-element model, periodic displacement BC's are applied such that all six components of the deformation are zero (seventh case in Table 10). The force and moment resultants are computed using one of the procedures described above. The thermal expansion coefficients α^p, and thermal bending coefficients β^p are then obtained from the relation:

$$\begin{Bmatrix} \alpha^p \\ \beta^p \end{Bmatrix} = -\frac{1}{T_0} \begin{bmatrix} A & B \\ B & D \end{bmatrix}^{-1} \begin{Bmatrix} N \\ M \end{Bmatrix} \tag{24}$$

3.4.3 Results for Plate Stiffness Coefficients

The plate $[A]$, $[B]$, $[D]$ matrices and CTE's were found for the seven examples listed in Table 2 by implementing the finite element code $\mu TE\chi$-20. The plate properties for the isotropic and bimaterial cases are presented in Tables 11 and 12 respectively. The bimaterial plate properties were also computed using the lamination theory for two plies, and from the 3-D elastic constants (Table 12). For example the coefficient D_{11} is obtained from the 3-D elastic constants as

$$D_{11} = \frac{E_x^M h^3}{12(1 - v_{xy}^{M^2})}$$

636

The finite element results for the bimaterial case were exact, *i.e,* identical to the results obtained with the two-ply lamination theory. The [A] and [D] matrices computed from the bimaterial 3-D constants were found to be in good agreement with the two-ply lamination theory only because both the layers were equal in thickness. In-general, however the plate properties obtained from the 3-D elastic constants would be different from the two-ply lamination theory results. The plate properties for the unidirectional composite examples are presented in Table 13 and for the textile examples in Table 14. In all the examples it was found that the plate properties, especially [B], D_{11}, $\{\alpha^p\}$ and $\{\beta^p\}$ could not be predicted from the corresponding 3-D elastic constants.

4. FINITE ELEMENT MODELS FOR STRENGTH PROPERTIES

In the previous sections, we had demonstrated methods to model a general textile composite either as a three-dimensional material or as a thin plate/beam to predict their corresponding thermo-mechanical coefficients. In this section we extend the same numerical models to compute the thermal residual stresses due to processing in the yarns and the matrix. Then the numerical models are used to study the strength behavior of the composite by predicting the failure envelopes for thin and thick textile composites.

4.1 Thermally Induced Residual Microstresses

The mismatch in the CTE's for the constituent materials in the composite induces the residual microstresses in the yarn and matrix. The difference between composite curing temperature and room temperature then serves as the driving force to create these microstresses. The microstresses in the vicinity of the yarn-matrix interface are particularly important as they could lead to failure due to debonding. Since composites designed for high temperature applications are fabricated at higher temperatures, the residual microstresses become particularly relevant in the strength considerations of such composites.

4.1.1 Determination of Residual Microstresses

Let T_o be the difference between room temperature and the composite fabrication temperature. Since the composite is stress free at the fabrication temperature, which is above the room temperature, T_o is generally negative. The residual microstresses in the yarn and the matrix are obtained by superposing the microstresses due to the two load cases as explained below. In the first load case, the unit-cell is constrained from expanding by fixing the corner nodes of the unit-cell and enforcing zero displacement difference between corresponding nodes on opposite faces of the unit-cell (periodic displacement BC's). A temperature difference T_o is applied to all elements in the finite element model. This is exactly the same problem we solve for finding the three-dimensional CTE's. The applied boundary conditions mean that all the macroscopic strain components are equal to zero ($\{\varepsilon^M\} = 0$, $\Delta T^M = T_0$). Then the corresponding macroscopic stresses required to restrain the unit-cell expansion are

given by

$$\{\sigma^M\} = -[C]\{\alpha^s\}T_o \qquad (26)$$

In the second load case, deformations are applied so as to reverse the macroscopic stresses developed in the first load case. This can be accomplished by imposing the deformations $\{\varepsilon^M\} = \{\alpha^s\}\ T_o$ and $\Delta T^M=0$. It can be noted that the macroscopic stresses developed in the second loading case $[C]\{\alpha^s\}T_o$ are equal and opposite to the macrostresses in Eqn. (26). The microstresses from both load cases are superposed to obtain the residual stresses due to free thermal expansion.

The same idea can be extended to finding the residual microstresses in the plate model. Then the deformations to be applied in the first load case are $\{\varepsilon^M\} = 0$, $\{\kappa^M\} = 0$ and $\Delta T^M = T_o$; and the deformations in the second load case are $\{\varepsilon^M\} = \{\alpha^p\}\ T_o$, $\{\kappa^M\} = \{\beta^p\}$ T_o and $\Delta T^M = 0$. The residual microstresses were computed for the plain-weave textile beam at the Gaussian center of the elements in the unit-cell. Figure 7 shows the thermal stress contours for σ_{xx}, σ_{zz} and τ_{xz}. The composite curing temperature was assumed to be 150°C above room temperature.

4.2 Strength Modeling of Textile Composites

There are many failure criteria or strength theories for unidirectional fiber composites. This for example includes (Agarwal and Broutman, 1990) maximum stress theory, maximum strain theory, Tsai-Hill theory. Even though failure of a material is a very complex phenomenon, engineering strength theories such as mentioned above have been found to be useful in design. The interpretation of strength values obtained from such theories are different for different materials. For example in metal matrix composites the failure envelope obtained using the above theories will correspond to the initial yield surface (Dvorak et al., 1973). In graphite/epoxy composites the failure theories can be used to predict fiber or matrix failure. In the present study our intent is to explore the possibility of developing such failure criteria for textile composites.

4.2.1 Determination of Composite Failure Envelope

Our approach is similar to that used by Dvorak et al. (1973). A state of homogeneous deformation, corresponding to each of the six macrostrain components, are independently applied to the unit-cell by imposing the boundary conditions explained in Section 3.1. For each case, the various stress components are computed in the elements in the unit-cell - typically at the element Gaussian integration points. These stresses will be referred to as microstresses. Assuming linear elastic behavior, the microstresses can be computed for any arbitrary combination of the macrostrain components. Since we know the macroscopic elastic constants, we can find a relation between microstresses at a point and any arbitrary state of

macrostress as:

$$\{\sigma\} = [F] \{\sigma^M\} \qquad (27)$$

[F] can be considered as a matrix of influence coefficients, which is evaluated at the integration points of all the elements in the unit-cell. We also assume that the failure behavior of the matrix material and the yarn is known. For instance, let the failure criterion of the matrix be given by $[H] \{\sigma\}_{matrix} = 1$. Then the failure criterion for the composite is obtained from Eqn. (27) as $[H] [F] \{\sigma^M\} = 1$. The same idea also applies for the yarn. The textile composite is assumed to have failed, if there is failure on the microscale in any one of the constituent materials - either matrix or the yarn. By varying the macrostresses using a numerical simulation, failure envelopes can be obtained for the idealized homogeneous material. It might be noted that Eqn. (27) can be modified to include the thermal residual stress field in the unit-cell as

$$\{\sigma\} = [F] \{\sigma^M\} - \{\sigma_T\} T_o \qquad (28)$$

where $\{\sigma_T\}$ is the matrix of thermal microstresses computed at the element integration point for a temperature difference of T_o.

4.2.2 Effect of Stress Gradients on Strength

The strength analysis for a three-dimensional composite can extended for thin composites using the plate model. As mentioned in Section 3.2, the macroscopic stresses will not be homogeneous thorough the thickness in such composites. Then the composite failure will be determined by the stress gradients through the thickness, represented by the averaged force resultants (F) and moment resultants (M). The composite failure criterion will be of the form

$$[H][F] \begin{Bmatrix} N \\ M \end{Bmatrix} = 1 \qquad (29)$$

Thus the failure envelope of the composite will be in the six-dimensional space of the force resultants and the moment resultants. The above procedure was demonstrated using the beam model, for the case of a plain-weave textile composite.

4.2.3 Beam Failure Envelope Results

The strength properties used for the constituent materials in the beam are as follows:
Yarn: σ_L^T=1725 MPa, σ_L^C=1366 MPa, σ_T^T=42 MPa, σ_T^C=230 MPa, τ_{LT}=95 MPa
Matrix: σ^T=70 MPa, σ^C=100 MPa
where the superscripts 'T' and 'C' refer to the tensile and compressive strengths respectively. The maximum principal stress criterion was used to determine the matrix failure and the maximum strain theory for unidirectional fiber composite was used for the yarn. Both continuum and structural failure envelopes were developed. Figures 8 and 9 depict the

structural failure envelopes in the *P-M* space. If we assume that the beam is made of a homogeneous but orthotropic material with properties as predicted by the continuum model, then one can derive structural failure envelopes from the continuum failure envelopes using simple beam theories. The derived structural failure envelopes are compared with that obtained from direct micromechanical analyses in Figs. 10 and 11 respectively. One can note that the continuum failure criteria are very conservative for the case of a thin beam.

5. ANALYTICAL MODELS FOR STIFFNESS PROPERTIES

The complex yarn architectures in a textile composite make numerical modeling of the unit-cell extremely difficult. Analytical methods are popular because they are easy to model and suitable for performing parametric analysis. However these methods are approximate because they assume a certain state of stress or strain in the unit-cell. Averaging the stiffness or compliances of the matrix and the inclusion has been used to estimate the bounds of effective elastic properties of the composite. Essentially the stiffness averaging assumes a state of uniform strain in the composite (isostrain), and compliance averaging assumes a state of uniform stress (isostress) in the matrix and inclusion. In fact the rule of mixtures expressions for estimating the effective properties of a unidirectional composite is based on such averaging schemes. These methods are too simplistic, because the state of stress/strain in a textile composite under a uniform macrostress is much more complex. We propose a scheme of selective averaging in which both stiffness and compliance coefficients can be averaged selectively depending on a more realistic assumption of either isostress or isostrain.

5.1 Selective Averaging Method (SAM)

Consider a rectangular parallelepiped of dimensions $a \times b \times c$ as the unit-cell. To find the first column of the effective stiffness matrix, the unit-cell is divided into slices (mesolevel) of thickness d parallel to the yz-plane (Fig. 12a). Each slice is further sub-divided into elements (microlevel) as shown in Figs. 12(b) and 12(c). In this section, to distinguish between the macrolevel, mesolevel and microlevel properties, an over-tilde is used to denote the mesolevel properties, and a superscript "M" is used to denote the macrolevel properties. For example, $[C^M]$, $[\tilde{C}]$ and $[C]$ will represent the macrolevel, mesolevel and microlevel stiffness respectively. The unit-cell is subjected to a deformation such that all macrostrains except ε_{xx}^M are equal to zero and $\varepsilon_{xx}^M = 1$. It is assumed that the mesolevel and microlevel strains, corresponding to the zero macrostrains, are negligible.

$$\epsilon_i^M = \tilde{\epsilon}_i = \epsilon_i = 0 \qquad i \neq 1 \tag{30}$$

The average stiffness of a slice can be obtained based on the isostrain assumption within the slice ($\varepsilon_{xx}(x,y,z) = \tilde{\varepsilon}_{xx}(x)$) as :

$$\tilde{C}_{11}(x) = \frac{1}{bc} \int\int C_{11}(x,y,z)\,dy\,dz \tag{31}$$

where $C_{11}(x,y,z)$ is the element stiffness coefficient transformed to the unit-cell coordinates. The stiffness of the slices are averaged on the macrolevel based on the isostress assumption, i.e., $\sigma_{xx}(x) = \sigma_{xx}^M$. Thus the first column of the effective stiffness matrix can be computed using the following relations:

$$\frac{1}{C_{11}^M} = \frac{1}{a}\int \frac{1}{\tilde{C}_{11}(x)}\,dx$$

$$\tag{32}$$

$$C_{i1}^M = \frac{1}{abc}\int\int\int \frac{C_{11}^M}{\tilde{C}_{11}(x)}\,C_{i1}(x,y,z)\,dx\,dy\,dz \quad (i=2,...,6)$$

A similar procedure can be implemented to determine the second and third columns of the homogenous stiffness matrix $[C^M]$.

A slightly different averaging scheme is used when the unit-cell is subjected to shear strains on the macrolevel. Consider the case where the unit-cell is subjected to unit γ_{yz}^M at macroscale. Assume that all the other components of strain at the macrolevel, mesolevel and microlevel are zero, i.e.,

$$\epsilon_i^M = \tilde{\epsilon}_i = \epsilon_i = 0 \qquad i \neq 4 \tag{33}$$

where $\epsilon_4 = \gamma_{yz}$. We also assume that the shear stress is constant in a slice such that $\tau_{yz}(x,y,z) = \tau_{yz}(x)$. The shear compliance of a slice can then be obtained by averaging the shear compliances of all the elements in the slice as:

$$\frac{1}{\tilde{C}_{44}(x)} = \frac{1}{bc}\int\int \frac{1}{C_{44}(x,y,z)}\,dy\,dz \tag{34}$$

The fourth column of the stiffness matrix C_{i4}^M is obtained under the assumption that all the slices are under a state of constant shear strain:

$$C_{i4}^M = \frac{1}{abc}\int\int\int \frac{\tilde{C}_{44}(x)}{C_{44}(x,y,z)}\,C_{i4}(x,y,z)\,dx\,dy\,dz \quad (i=1,...,6) \tag{35}$$

A similar procedure is used to determine the fifth and sixth columns of $[C^M]$.

A code was written in FORTRAN to implement SAM. The code ($\mu TE\chi$-10) was used to predict the elastic constants for the seven examples, whose constituent material properties are listed in Table 2. Input to the code were the unit-cell dimensions, yarn/fiber geometry, constituent material properties, and the number of divisions required to discretize the unit-cell in the x, y and z directions. The element stiffness matrix [C] was computed by finding the constitutive stiffness matrix for the point at the center of the element, and transforming it to the unit-cell coordinate system.

The results for the bimaterial medium (example 2) are given in Table 15. The bimaterial medium consisted of two layers of isotropic materials stacked alternately in the z-direction (Fig. 1). It can be observed that SAM marginally under-predicts the bimaterial longitudinal and transverse Youngs moduli, while the inplane and transverse shear moduli are exact. Table 16 presents the SAM results for two cases of unidirectional composite (examples 3 and 4). The fiber and matrix had identical poisson ratios in example 3, and different poisson ratios in example 4. The elastic constants from SAM were compared with the finite element results from Section 3.1 and with analytical solutions for a unidirectional composite (the rule of mixtures formulae and the Halpin-Tsai equations). Table 17 compares the SAM properties for three textile composites (examples 5, 6 and 7) with the previously computed finite element results and other available results. In all three cases the elastic constants obtained by implementing SAM were in good agreement with the available results.

6. CONCLUSIONS

Micromechanical models were demonstrated to predict the stiffness and strength behavior of textile composites. In thin textile composites, the stress gradients through the thickness were significant, and hence the composite was modeled as a homogeneous plate/beam rather than homogeneous continua. The beam model was first discussed to present the issues involved in computing the structural stiffness and strength properties. Then the plate model was presented for computing the plate stiffness and plate CTE's, and to predict the failure envelope for a thin textile composite. The failure envelope for a thin textile composite was described in the space of the force and moment resultants instead of the space of the macroscopic stresses. It was shown for various examples, that the plate properties could not be predicted from the corresponding continuum properties.

In the models using finite elements (Section 3), the periodic BC's were enforced for continuity of tractions and displacements across the unit-cell boundaries. Therefore the finite element results for the stiffness properties could be expected to be very accurate. However due to difficulties in mesh generation, the unit-cell for the 3-D continuum and the plate models were discretized into inhomogeneous finite elements (elements with one or more constituent materials). Thus the stresses in the vicinity of the yarn-matrix interface for the above models may be approximate. For the beam model, however, the unit-cell was

discretized into homogeneous elements.

The Selective Averaging Method (SAM) discussed in Section 6 was based on a combination of isostress and isostrain assumptions. The method was fast and easy to implement and suitable for parametric studies such as yarn preform selection. Extension of SAM to predict the continuum CTE's, plate stiffness and plate CTE's is straightforward and is underway.

REFERENCES

Agarwal, D. A.; and Broutman, L. J.: *Analysis and Performance of Fiber Composites.* John Wiley and Sons Pub., 1990.

Cook, R. D.; Malkus, D. S.; and Plesha, M. E.: *Concepts and Applications of Finite Element Analysis.* John Wiley and Sons Pub. Third Edition, 1989, pp. 272-274.

Dasgupta, A.; Bhandarkar, S.; Pecht, M.; and Barkar, D.: Thermo-elastic Properties of Woven-fabric Composites using Homogenization Techniques. *Proceedings of the American Society for Composites. Fifth Technical Conference.*, 1990, pp. 1001-1010.

Dvorak, G. J.; Rao, M. S. M.; and Tarn, J. Q.: Yielding in Unidirectional Composites under External Loads and Temperature Changes. *J. Comp. Materials*, 1973, Vol.7, pp. 194-216.

Halpin, J. C.; and Tsai, S. W.: Effects of Environmental Factors on Composite Materials. *AFML-TR -67-423*, June 1969.

Ishikawa, T.; and Chou, T. W.: Elastic Behavior of Woven Hybrid Composites. *J. Comp. Mater.*, 1982, Vol. 16, pp. 2-19.

Ishikawa, T.; and Chou, T. W.: One Dimensional Mircomechanical Analysis of Woven Fabric Composites. *AIAA J.*, 1983a, Vol. 21, pp. 1714-1721.

Ishikawa, T.; and Chou, T. W.: In-plane Thermal Expansion and Thermal Bending Coefficients of Fabric Composites. *J. Comp. Mater.*, 1983b, Vol. 17, pp. 92-104.

Ma, C. L.; Yang, J. M.; and Chou, T. W.: Elastic Stiffness of Three Dimensional Braided Textile Structural Composites. *Composite Materials: Testing and Design (Seventh Conference)*, ASTM STP 893, 1986, pp. 404-421.

Marrey, R. V.; and Sankar, B. V.: Stress Gradient Effects on Stiffness and Strength of Textile Structural Composites. *Composite Materials and Structures, 1993 ASME Winter Annual Meeting,* AD-Vol. 37/AMD-Vol. 179, 1993a, pp. 133-148.

Marrey, R. V.; and Sankar, B. V.: Thermo-mechanical Properties of and Residual Stresses in

Textile Structural Composites. *Proc. Am. Soc. Composites. VIII Tech. Conference* , 1993b, pp. 499-508.

Naik, R. A.: Analysis of Woven and Braided Fabric Reinforced Composites. NASA CR-194930, 1994.

Sankar, B. V.; and Marrey, R. V.: A Unit-cell Model of Textile Composite Beams for Predicting Stiffness Properties. *Composites Science and Technology*, 1993, Vol. 49, pp. 61-69.

Whitcomb, J. D.: Three Dimensional Stress Analysis of Plain Weave Composites. *Composite Materials Fatigue and Fracture (Third Volume)*, ASTM STP 1110, 1991, pp. 417-438.

Whitney, J. M.: Shear Correction Factors for Orthotropic Laminates under Static Load. *J. Appl. Mech.*, 1973, Vol. 40, pp. 302-304.

Yang, J. M.; and Chou, T. W.: Performance Maps of Textile Structural Composites. *Sixth International Conference on Composite Materials (ICCM VI).*, 1987, Vol. 5 , pp. 579-588.

Yoshino, T.; and Ohtsuka, T., 1982: Inner Stress Analysis of Plane Woven Fiber Reinforced Plastic Laminates. *Bulletin of the JSME*, Vol. 25-202, pp. 485-492.

Table 1. Non-zero BC's Imposed to Obtain 3-D Thermo-Elastic Constants

stiffness coefficients to be obtained	non-zero BC's
first column of $[C]$ ($\varepsilon_{11}^M = 1$)	$u_1(L_1, x_2, x_3) - u_1(0, x_2, x_3) = L_1$
second column of $[C]$ ($\varepsilon_{22}^M = 1$)	$u_2(x_1, L_2, x_3) - u_2(x_1, 0, x_3) = L_2$
third column of $[C]$ ($\varepsilon_{33}^M = 1$)	$u_3(x_1, x_2, L_3) - u_3(x_1, x_2, 0) = L_3$
fourth column of $[C]$ ($\gamma_{23}^M = 1$)	$u_2(x_1, x_2, L_3) - u_2(x_1, x_2, 0) = L_3/2$ $u_3(x_1, L_2, x_3) - u_3(x_1, 0, x_3) = L_2/2$
fifth column of $[C]$ ($\gamma_{13}^M = 1$)	$u_1(x_1, x_2, L_3) - u_1(x_1, x_2, 0) = L_3/2$ $u_3(L_1, x_2, x_3) - u_3(0, x_2, x_3) = L_1/2$
sixth column of $[C]$ ($\gamma_{12}^M = 1$)	$u_1(x_1, L_2, x_3) - u_1(x_1, 0, x_3) = L_2/2$ $u_2(L_1, x_2, x_3) - u_2(0, x_2, x_3) = L_1/2$
CTE's ($\Delta T^M = 1$)	$\Delta T = 1$

Table 2. Properties of Constituent Materials for Examples 1-7

Example 1		
		$E = 10\ GPa,\ \nu=0.3,\ \alpha=10x10^{-6}/\,^{\circ}C$
	unit-cell size:	$0.500\times0.500\times0.256\ mm$
Example 2	layer 1 (E-glass):	$E_1=70\ GPa,\ \nu_1=0.200,\ \alpha_1=5x10^{-6}/\,^{\circ}C,\ V_1=0.5$
	layer 2 (epoxy):	$E_2=3.50\ GPa,\ \nu_2=0.350,\ \alpha_2=60x10^{-6}/\,^{\circ}C,\ V_2=0.5$
	unit-cell size:	$0.500\times0.500\times0.256\ mm$
Example 3	fiber:	$E_f=100\ GPa,\ \nu_f=0.300,\ \alpha_f=10x10^{-6}/\,^{\circ}C,\ V_f=0.6$
	matrix:	$E_m=10\ GPa,\ \nu_m=0.300,\ \alpha_m=100x10^{-6}/\,^{\circ}C$
	unit-cell size:	$10\times10\times10\ \mu m$
Example 4	fiber (E-glass):	$E_f=70\ GPa,\ \nu_f=0.200,\ \alpha_f=5x10^{-6}/\,^{\circ}C,\ V_f=0.6$
	matrix (epoxy):	$E_m=3.50\ GPa,\ \nu_m=0.350,\ \alpha_m=60x10^{-6}/\,^{\circ}C$
	unit-cell size:	$10\times10\times10\ \mu m$

Example 5
yarn properties (glass-epoxy):
$E_L=58.61\ GPa,\ E_T=14.49\ GPa,\ G_{LT}=5.38\ GPa,\ \nu_{LT}=0.250$
$\nu_{TT}=0.247,\ \alpha_L=6.15x10^{-6}/\,^{\circ}C,\ \alpha_T=22.64x10^{-6}/\,^{\circ}C,\ V_f=0.26$
matrix properties (epoxy):
$E=3.45\ GPa,\ \nu=0.37,\ \alpha=69x10^{-6}/\,^{\circ}C$
unit-cell size: $\qquad$ $1.680\times1.680\times0.228\ mm$

Examples 6, 7
yarn properties (graphite-epoxy):
$E_L=144.80\ GPa,\ E_T=11.73\ GPa,\ G_{LT}=5.52\ GPa,\ \nu_{LT}=0.230$
$\nu_{TT}=0.300,\ \alpha_L=-0.324x10^{-6}/\,^{\circ}C,\ \alpha_T=14.00x10^{-6}/\,^{\circ}C,\ V_f=0.64$
matrix properties (epoxy):
$E=3.45\ GPa,\ \nu=0.35,\ \alpha=40x10^{-6}/\,^{\circ}C$
unit-cell size: $\qquad$ $2.822\times2.822\times0.2557\ mm$ (Example 6)
$\qquad\qquad\qquad\quad$ $7.055\times7.055\times0.2557\ mm$ (Example 7)

Table 3. 3-D Properties for Examples 1 and 2 using Finite Elements

		E_x, E_y (GPa)	E_z (GPa)	G_{xz}, G_{yz} (GPa)	G_{xy} (GPa)	ν_{xz}, ν_{yz}	ν_{xy}	$\alpha_x^s, \alpha_y^s \times 10^{-6}/^\circ C$	$\alpha_z^s \times 10^{-6}/^\circ C$
Example 1 (isotropic medium)	$\mu TE\chi$-20 (FEA)	10	10	3.85	3.85	0.300	0.300	10	10
	exact solution	10	10	3.85	3.85	0.300	0.300	10	10
Example 2 (bimaterial medium)	$\mu TE\chi$-20 (FEA)	36.79	9.79	2.48	15.23	0.312	0.208	8.19	59.60
	exact solution	36.79	9.79	2.48	15.23	0.312	0.208	8.19	59.60

Table 4. 3-D Properties for Examples 3 and 4 using Finite Elements

		E_L (GPa)	E_T (GPa)	G_{LT} (GPa)	G_{TT} (GPa)	ν_{LT}	ν_{TT}	$\alpha_L \times 10^{-6}/^\circ C$	$\alpha_T \times 10^{-6}/^\circ C$
Example 3 (unidirect. composite)	$\mu TE\chi$-20 (FEA)	63.55	36.48	12.93	9.94	0.300	0.232	15.74	40.79
	rule of mixt./ Halpin-Tsai eqns.	64	34.55	11.26	-	0.300	0.300	15.63	55.11
Example 4 (unidirect. composite)	$\mu TE\chi$-20 (FEA)	43.12	18.15	5.59	3.92	0.242	0.222	7.40	25.44
	rule of mixt./ Halpin-Tsai eqns.	43.40	14.79	4.45	-	0.260	0.252	6.77	34.24

Table 5. 3-D Properties for Examples 5, 6 and 7 using Finite Elements

		E_x, E_y (GPa)	E_z (GPa)	G_{xz}, G_{yz} (GPa)	G_{xy} (GPa)	ν_{xz}, ν_{yz}	ν_{xy}	$\alpha_x^s, \alpha_y^s x$ $10^{-6}/°C$	$\alpha_z^s x$ $10^{-6}/°C$
Example 5 (plain-weave)	$\mu TE\chi$-20 (FEA)	11.55	6.26	1.94	2.12	0.399	0.186	29.75	75.82
	Dasgupta results	14.38	6.25	1.94	3.94	0.463	0.167	22.5	86
Example 6 (plain-weave)	$\mu TE\chi$-20 (FEA)	58.27	10.92	4.32	4.84	0.363	0.097	1.47	23.15
	TEXCAD	64.38	11.49	5.64	4.87	0.396	0.027	1.33	20.71
Example 7 (5-harness weave)	$\mu TE\chi$-20 (FEA)	62.51	11.02	4.45	4.80	0.349	0.047	1.58	23.18
	TEXCAD	66.33	11.51	4.93	4.89	0.342	0.034	1.46	21.24

Table 6. Periodic Displacement BC's for Beam Stiffness Coefficients

	$u(L,z)-u(0,z)$	$w(L,z)-w(0,z)$	ΔT
Case i. unit axial strain $(\varepsilon_0^M=1)$	L	0	0
Case ii. unit curvature $(\kappa^M=1)$	Lz	$-L^2/2$	0
Case iii. unit shear strain $(\gamma_0^M=1)$	0	L	0

Table 7. Constituent Material Properties for Beam Examples

isotropic beam	$E = 10$ GPa, $\nu = 0.30$, $\alpha = 10 \times 10^{-6}$ /°C
bimaterial beam	$E_1 = 70$ GPa, $\nu_1 = 0.33$, $\alpha_1 = 23 \times 10^{-6}$ /°C $E_2 = 3.5$ GPa, $\nu_2 = 0.35$, $\alpha_2 = 60 \times 10^{-6}$ /°C
plain-weave textile beam	**yarn:** $E_1 = 159$ GPa, $E_2 = 10.9$ GPa, $G_{12} = 6.4$ GPa, $\nu_{12} = 0.38$, $\nu_{23} = 0.38$, $\alpha_1 = 0.045 \times 10^{-6}$ /°C, $\alpha_2 = 20.2 \times 10^{-6}$ /°C where the yarn direction is parallel to the 1-axis and 23-plane is the plane of isotropy. **matrix:** $E_m = 3.5$ GPa, $\nu_m = 0.35$, $\alpha_m = 60 \times 10^{-6}$ /°C.

Table 8. Comparison of Beam Stiffness Coefficients and CTE's (SI Units)

		K_{11}	K_{12}	K_{22}	K_{33}	α_P /°C	α_M /°C
isotropic beam	unit-cell analysis	19.78×10^6	0	5.35	5.96×10^6	10×10^{-6}	0
	beam theory	19.78×10^6	0	5.34	5.77×10^6	10×10^{-6}	0
bimaterial beam	unit-cell analysis	74.29×10^6	30.20×10^3	20.06	8.47×10^6	30.73×10^{-6}	-14.62×10^{-3}
	beam theory	74.29×10^6	30.20×10^3	20.06	8.62×10^6	30.74×10^{-6}	-14.63×10^{-3}
plain-weave textile beam	unit-cell analysis	27.76×10^6	0	5.41	9.21×10^6	12.66×10^{-6}	-24.12×10^{-6}
	mosaic model	71.48×10^{-6}	0	8.13	8.14×10^6	4.39×10^{-6}	0

K_{13}, K_{23} and α_V are zero for all cases

Table 9. Comparison of Beam CTE's for Plain-weave Textile Beam

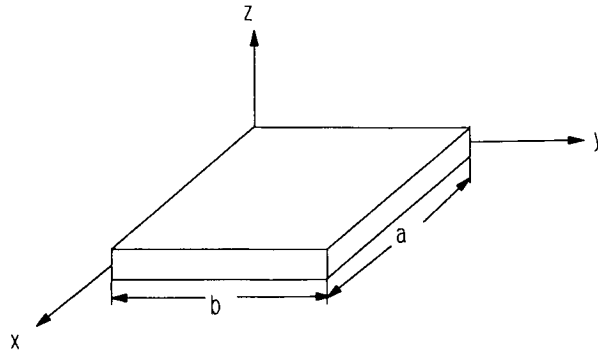|	CTE's from beam model	CTE's from continuum model	% error
$\alpha_P \times 10^{-6}$ °/C	12.66	11.30	-10.46
$\alpha_M \times 10^{-6}$ °/C/m	-24.12	0	100
α_V °/C	0	0	-

Table 10. Periodic Displacement BC's Imposed on the Lateral Faces of the Plate Unit-cell

		$u(a,y)-$ $u(0,y)$	$v(a,y)-$ $v(0,y)$	$w(a,y)-$ $w(0,y)$	$u(x,b)-$ $u(x,0)$	$v(x,b)-$ $v(x,0)$	$w(x,b)-$ $w(x,0)$	ΔT
1.	$\varepsilon_{x0}^{M}=1$	a	0	0	0	0	0	0
2.	$\varepsilon_{y0}^{M}=1$	0	0	0	0	b	0	0
3.	$\gamma_{xy0}^{M}=1$	0	a/2	0	b/2	0	0	0
4.	$\kappa_{x}^{M}=1$	az	0	$-a^2/2$	0	0	0	0
5.	$\kappa_{y}^{M}=1$	0	0	0	0	bz	$-b^2/2$	0
6.	$\kappa_{xy}^{M}=1$	0	az/2	-ay/2	bz/2	0	-bx/2	0
7.	$\Delta T^{M}=1$	0	0	0	0	0	0	1

Table 11. Non-zero $[A]$, $[B]$ and $[D]$ Coefficients for Example 1 (Isotropic Plate) using Finite Elements

	A_{11} x10^6	A_{12} x10^6	A_{22} x10^6	A_{66} x10^6	D_{11} x10^{-3}	D_{12} x10^{-3}	D_{22} x10^{-3}	D_{66} x10^{-3}	α_x^p, α_y^p x10^{-6}/°C
$\mu TE\chi$-20 (FEA)	2.810	0.843	2.810	0.983	15.320	4.606	15.320	5.358	10
lamination theory	2.810	0.843	2.810	0.983	15.310	4.593	15.310	5.358	10

$[A]$, $[B]$ and $[D]$ coefficients in SI units

Table 12. Non-zero $[A]$, $[B]$ and $[D]$ Coefficients for Example 2 (Bimaterial Plate) using Finite Elements

	A_{11}, A_{22} x10^6	A_{12} x10^6	A_{66} x10^6	B_{11}, B_{22} x10^3	B_{12} x10^3	B_{66} x10^{-3}
$\mu TE\chi$-20 (FEA)	9.832	2.043	3.895	- 0.563	- 0.108	- 0.228
lamination theory for two plies	9.832	2.043	3.895	- 0.563	- 0.108	- 0.228
lamination theory using 3-D elastic constants	9.844	2.048	3.899	0	0	0

	D_{11}, D_{22} x10^{-3}	D_{12} x10^{-3}	D_{66} x10^{-3}	α_x^p, α_y^p x10^{-6} /°C	β_x^p, β_y^p /°C/m
$\mu TE\chi$-20 (FEA)	53.590	11.149	21.220	17.800	0.170
lamination theory for two plies	53.573	11.131	21.220	17.814	0.170
lamination theory using 3-D elastic constants	53.762	11.183	21.293	8.190	0

Table 13. Non-zero [A], [B] and [D] Coefficients for Examples 3 and 4 (Unidirectional Composite) using Finite Elements

		A_{11} x10^6	A_{12} x10^6	A_{22} x10^6	A_{66} x10^6
Example 3	$\mu TE\chi$-20 (FEA)	0.690	0.149	0.496	0.177
	Halpin-Tsai eqns. and lamination theory	0.673	0.109	0.363	0.113
Example 4	$\mu TE\chi$-20 (FEA)	0.452	0.062	0.285	0.114
	Halpin-Tsai eqns. and lamination theory	0.444	0.039	0.151	0.045

		D_{11} x10^{-6}	D_{12} x10^{-6}	D_{22} x10^{-6}	D_{66} x10^{-6}	α_x^Px 10^{-6}	α_y^Px 10^{-6}
Example 3	$\mu TE\chi$-20 (FEA)	3.589	0.596	1.980	0.947	15.489	26.184
	Halpin-Tsai eqns. and lamination theory	5.606	0.908	3.026	0.939	15.625	55.112
Example 4	$\mu TE\chi$-20 (FEA)	2.256	0.224	0.873	0.568	7.378	13.188
	Halpin-Tsai eqns. and lamination theory	3.702	0.328	1.262	0.371	6.774	34.239

[A], [B] and [D] coefficients in SI units

Table 14. Non-zero $[A]$, $[B]$ and $[D]$ Coefficients for Examples 5, 6 and 7 using Finite Elements

		A_{11}, A_{22} x10^6	A_{12} x10^6	A_{66} x10^6	B_{11} x10^3
Example 5	$\mu TE\chi$-20 (FEA)	2.630	0.598	0.511	0
	lamination theory using 3-D constants	2.728	0.508	0.483	0
Example 6	$\mu TE\chi$-20 (FEA)	12.750	3.332	1.237	0
	lamination theory using 3-D constants	15.040	1.461	1.237	0
Example 7	$\mu TE\chi$-20 (FEA)	15.362	1.065	1.228	0.515*
	lamination theory using 3-D constants	16.020	0.756	1.228	0

		D_{11}, D_{22} x10^{-3}	D_{12} x10^{-3}	D_{66} x10^{-3}	α_x^p, α_y^p x10^{-6} /°C	β_x^p /°C/m
Example 5	$\mu TE\chi$-20 (FEA)	8.564	1.555	2.142	28.310	0
	lamination theory using 3-D constants	11.816	2.203	2.093	29.752	0
Example 6	$\mu TE\chi$-20 (FEA)	53.912	0.413	4.421	1.418	0
	lamination theory using 3-D constants	81.948	7.962	6.740	1.471	0
Example 7	$\mu TE\chi$-20 (FEA)	107.390	2.072	5.814	2.191	-0.018*
	lamination theory using 3-D constants	87.283	4.122	6.691	1.580	0

* In example 7, $B_{22} = -B_{11}$ and $\beta_y^p = -\beta_x^p$

$[A]$, $[B]$ and $[D]$ coefficients in SI units

Table 15. SAM Results for Examples 1 and 2

		E_x, E_y (GPa)	E_z (GPa)	G_{xz}, G_{yz} (GPa)	G_{xy} (GPa)	ν_{xz}, ν_{yz}	ν_{xy}
Example 2 (bimaterial medium)	$\mu TE\chi$-10 (SAM)	36.03	8.72	2.48	15.23	0.599	0.183
	exact solution	36.79	9.79	2.48	15.23	0.312	0.208

Table 16. SAM Results for Examples 3 and 4

		E_L (GPa)	E_T (GPa)	G_{LT} (GPa)	G_{TT} (GPa)	ν_{LT}	ν_{TT}
Example 3 (unidirectional composite)	$\mu TE\chi$-10 (SAM)	64	40.51	11.17	8.36	0.245	0.300
	$\mu TE\chi$-20 (FEA)	63.55	36.48	12.93	9.94	0.300	0.233
	rule of mixt./Halpin-Tsai eqns.	64	34.55	11.26	-	0.300	0.300
Example 4 (unidirectional composite)	$\mu TE\chi$-10 (SAM)	43.23	22.11	4.43	3.06	0.159	0.237
	$\mu TE\chi$-20 (FEA)	43.12	18.15	5.59	3.92	0.242	0.222
	rule of mixt./Halpin-Tsai eqns.	43.40	14.79	4.45	-	0.260	0.252

Table 17. SAM Results for Examples 5, 6 and 7

		E_x, E_y (GPa)	E_z (GPa)	G_{xz}, G_{yz} (GPa)	G_{xy} (GPa)	ν_{xz}, ν_{yz}	ν_{xy}
Example 5 (plain-weave)	$\mu TE\chi$-10 (SAM)	11.52	6.48	1.60	1.60	0.396	0.171
	$\mu TE\chi$-20 (FEA)	11.55	6.26	1.94	2.12	0.399	0.186
	Dasgupta results	14.38	6.25	1.94	3.94	0.463	0.167
Example 6 (plain-weave)	$\mu TE\chi$-10 (SAM)	64.49	11.37	3.97	4.26	0.398	0.027
	$\mu TE\chi$-20 (FEA)	58.27	10.92	4.32	4.84	0.378	0.098
	TEXCAD	64.38	11.49	5.64	4.87	0.396	0.027
Example 7 (5-harness weave)	$\mu TE\chi$-10 (SAM)	65.61	11.14	3.66	4.44	0.363	0.032
	$\mu TE\chi$-20 (FEA)	62.51	11.02	4.45	4.80	0.349	0.047
	TEXCAD	66.33	11.51	4.93	4.89	0.342	0.034
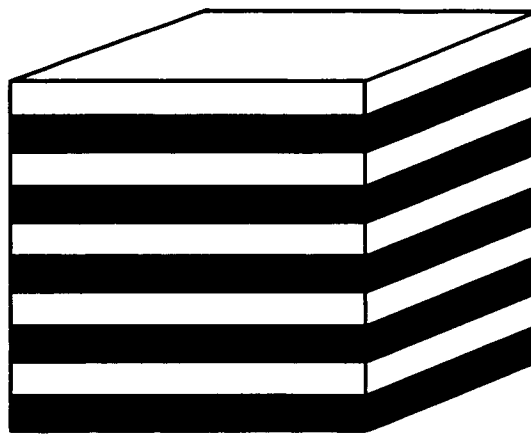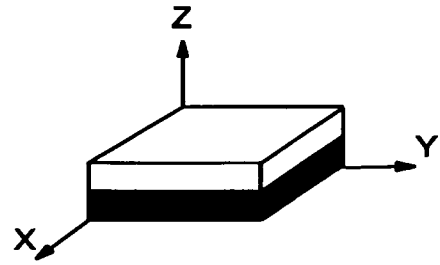
Figure 1. (a) bimaterial medium; (b) bimaterial unit-cell.
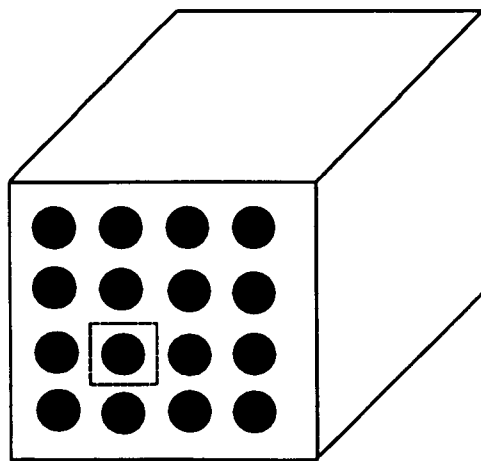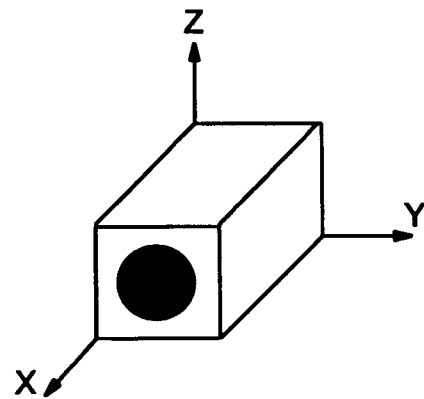
Figure 2. (a) unidirectional composite; (b) unit-cell for the composite.
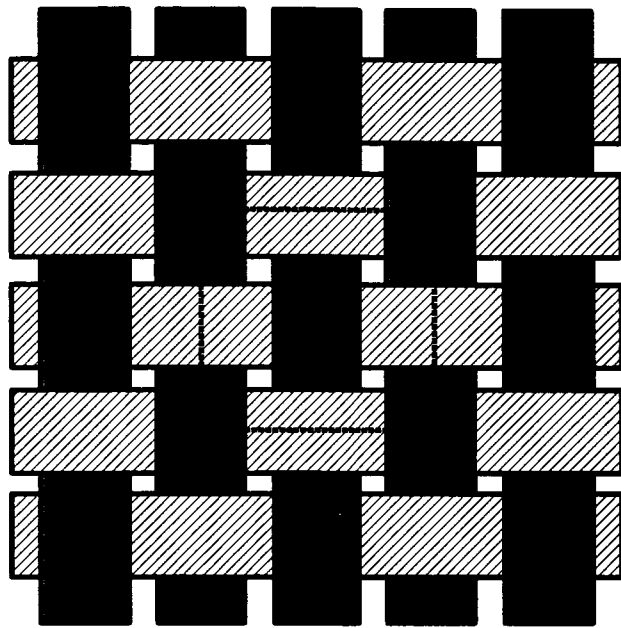
Figure 3. Yarn pattern in a plain weave preform (unit-cell boundary in dotted lines).
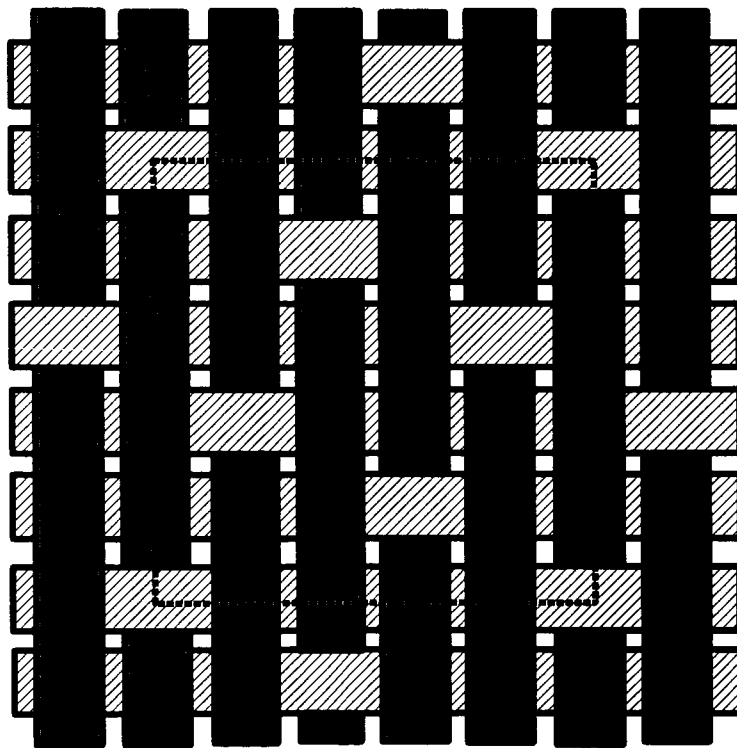
Figure 4. Yarn pattern in a 5-harness satin weave preform (unit-cell boundary in dotted lines).

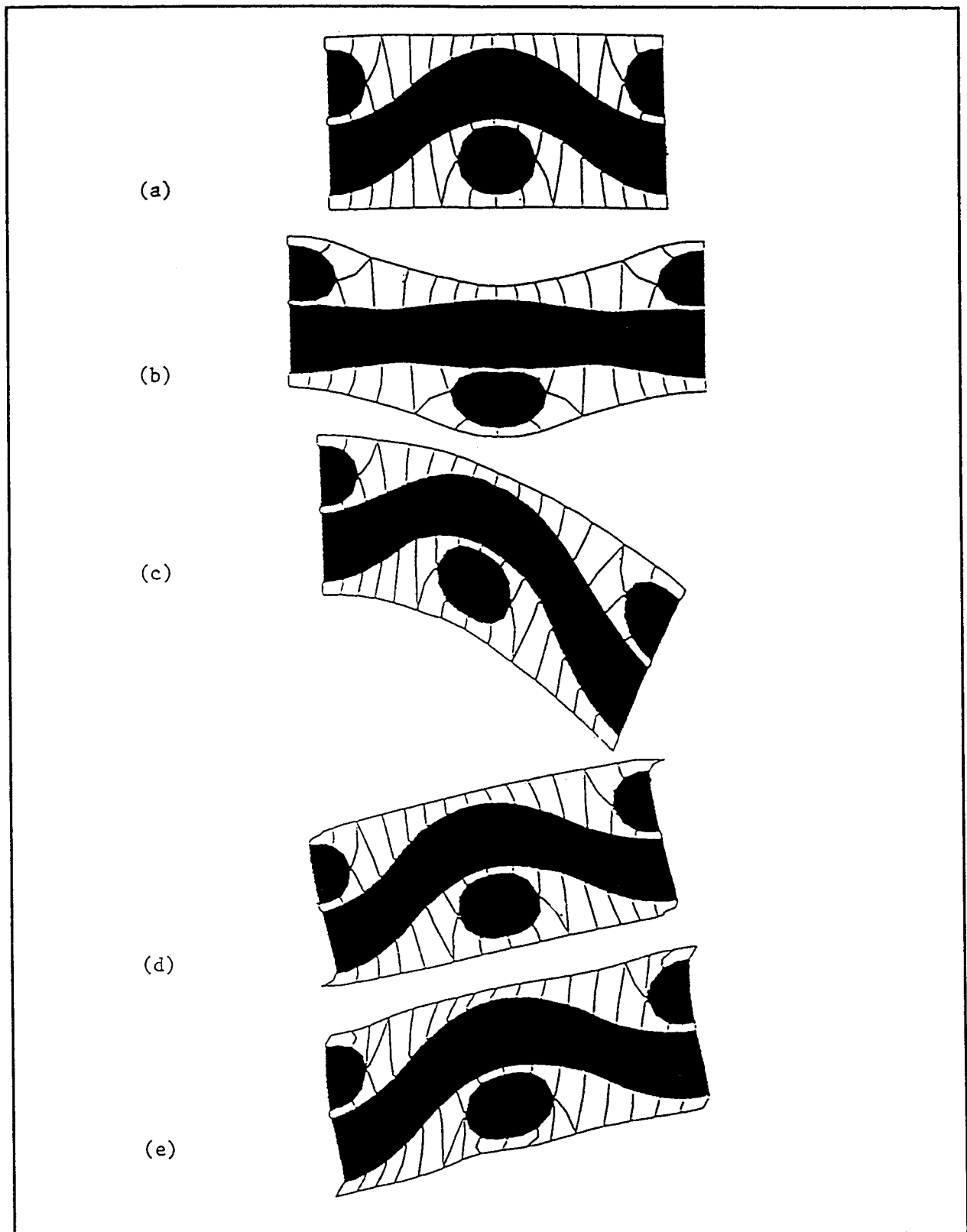657
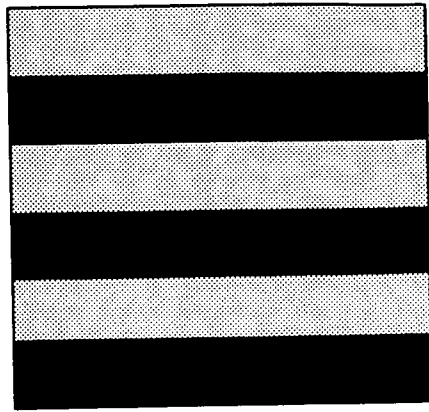
Figure 5. (a) Layered medium; (b) bimaterial beam.

Figure 6. Textile beam: (a) undeformed unit-cell and deformation under: (b) unit extensional strain; (c) unit curvature; (d) unit shear strain, top and bottom surfaces are traction free; (e) unit shear strain, tractions allowed on top and bottom surfaces. (not to scale)
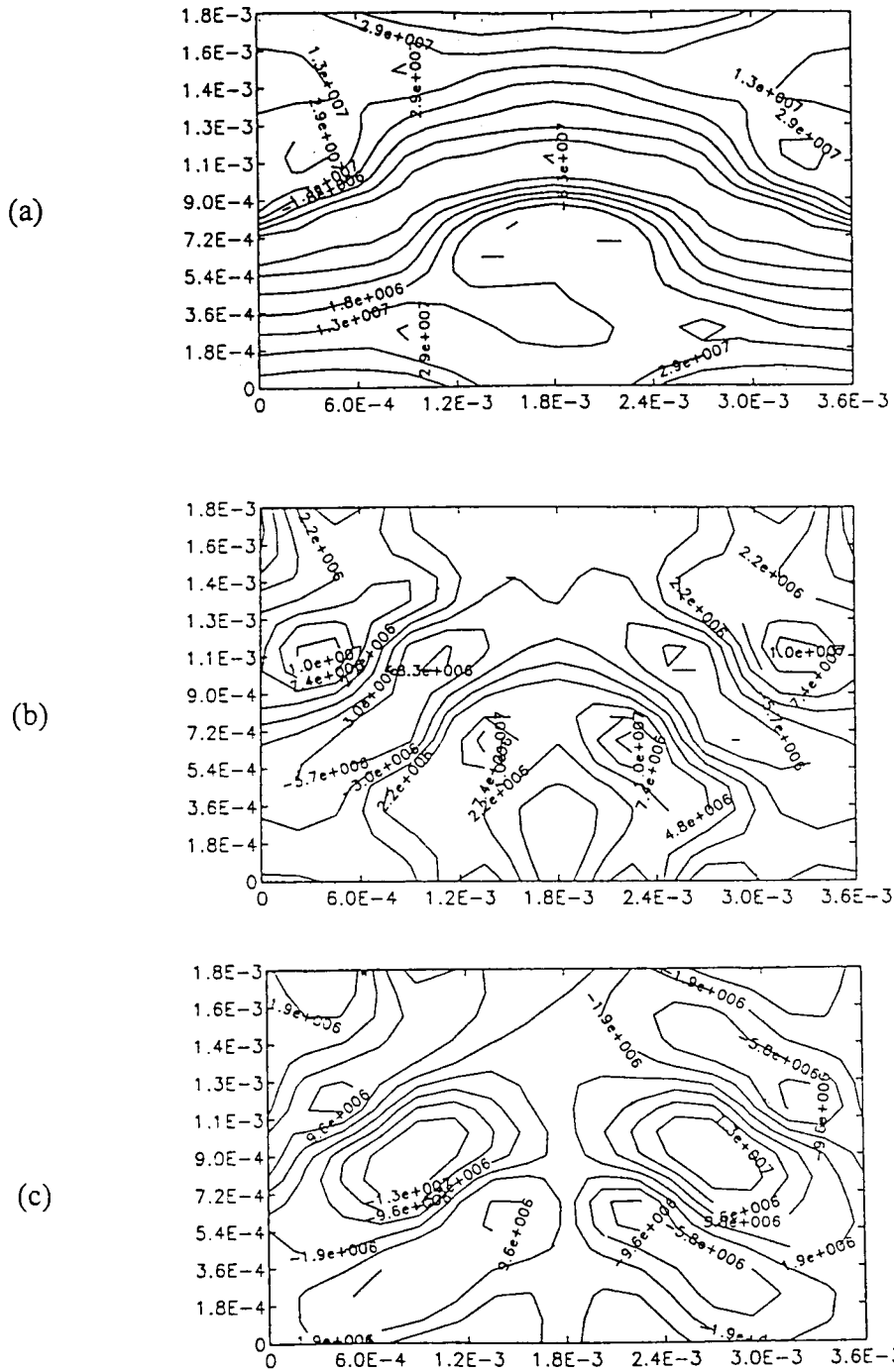
Figure 7. Thermal microstress contours in a plain weave beam for $\Delta T = -150^\circ C$: (a) σ_{xx}; (b) σ_{zz}; (c) τ_{xz}.
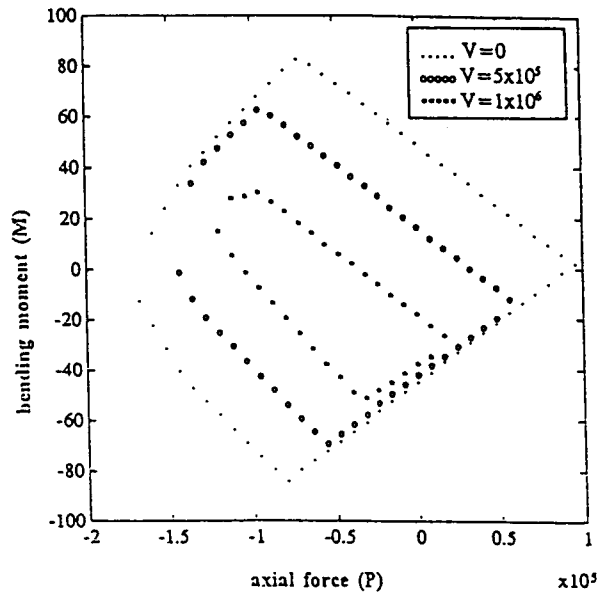
Figure 8. Beam failure envelope based on yarn failure.
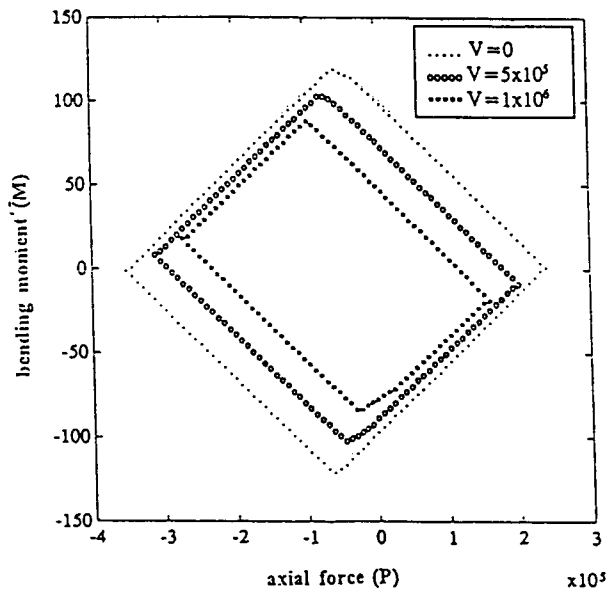
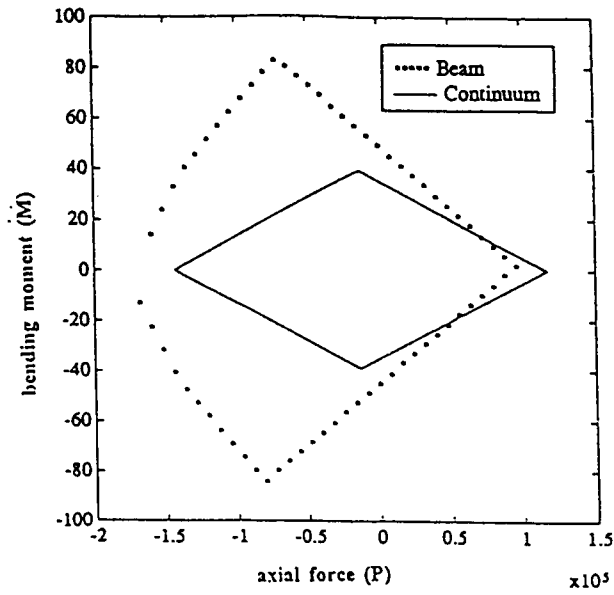**Figure 9.** Beam failure envelope based on matrix failure.

661

Figure 10. Comparison of failure envelopes based on yarn failure.
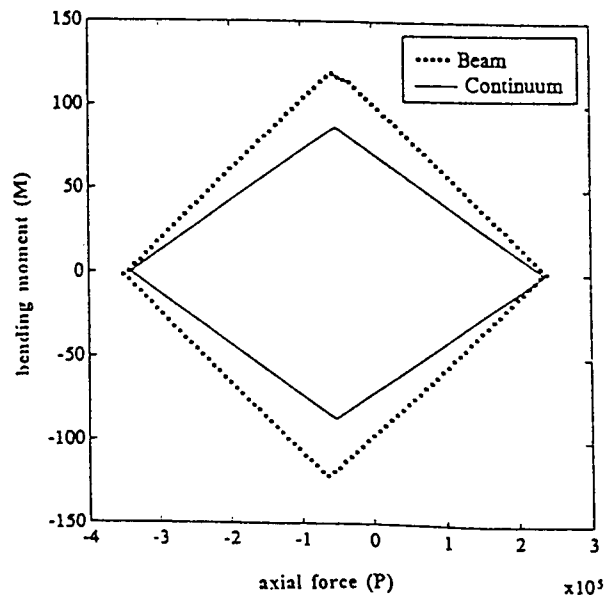

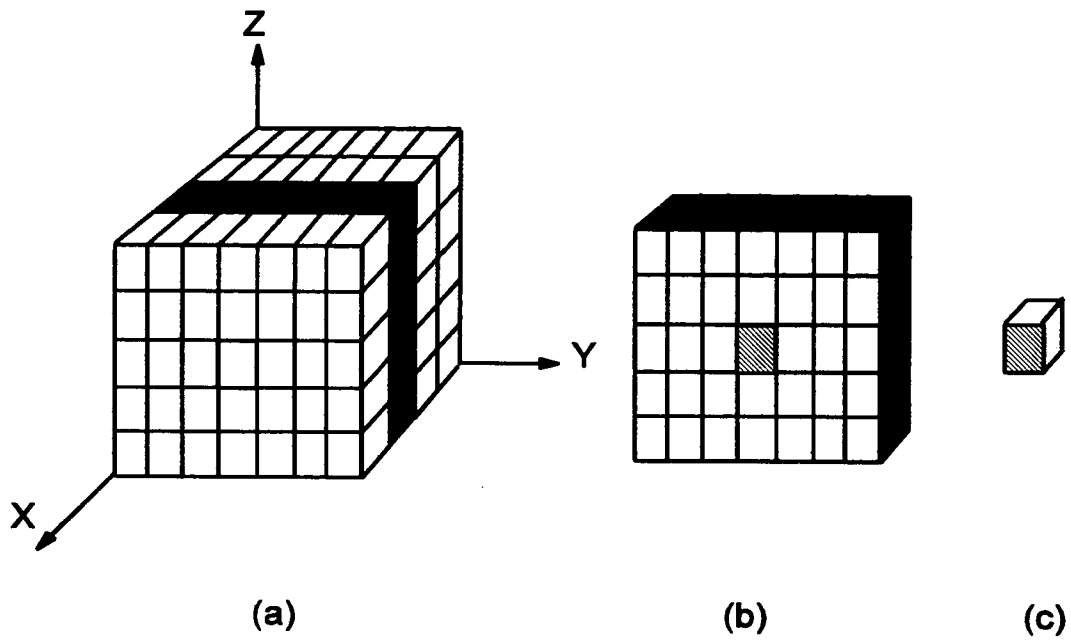**Figure 11.** Comparison of failure envelopes based on matrix failure.

Figure 12. Hierarchy of discretization for a unit-cell to implement SAM: (a) unit-cell (macrolevel); (b) slice (mesolevel); (c) element (microlevel).